



Laser microdissection of the alveolar duct enables single-cell genomic analysis

Robert D. Bennett¹, Alexandra B. Ysasi¹, Janeil M. Belle¹, Willi L. Wagner², Moritz A. Konerding², Paul C. Blainey³, Saumyadipta Pyne^{4*} and Steven J. Mentzer¹

¹ Laboratory of Adaptive and Regenerative Biology, Brigham and Women's Hospital, Harvard Medical School, Boston, MA, USA

² Institute of Functional and Clinical Anatomy, University Medical Center of the Johannes Gutenberg-University, Mainz, Germany

³ Broad Institute of Massachusetts Institute of Technology, Harvard University, Cambridge, MA, USA

⁴ CR Rao Advanced Institute of Mathematics, Statistics and Computer Science, Hyderabad, India

Edited by:

Tomer Kalisky, Bar-Ilan University, Israel

Reviewed by:

Thomi Brunner, University of Konstanz, Germany
Bernd E. R. Nuernberg, University of Tuebingen Hospitals and Clinics, Germany

*Correspondence:

Saumyadipta Pyne, University of Hyderabad Campus, Prof. CR Rao Road, Hyderabad, AP 500046, Telangana, India
e-mail: spyne@crraoaimscs.res.in

Complex tissues such as the lung are composed of structural hierarchies such as alveoli, alveolar ducts, and lobules. Some structural units, such as the alveolar duct, appear to participate in tissue repair as well as the development of bronchioalveolar carcinoma. Here, we demonstrate an approach to conduct laser microdissection of the lung alveolar duct for single-cell PCR analysis. Our approach involved three steps. (1) The initial preparation used mechanical sectioning of the lung tissue with sufficient thickness to encompass the structure of interest. In the case of the alveolar duct, the precision-cut lung slices were 200 μm thick; the slices were processed using near-physiologic conditions to preserve the state of viable cells. (2) The lung slices were examined by transmission light microscopy to target the alveolar duct. The air-filled lung was sufficiently accessible by light microscopy that counterstains or fluorescent labels were unnecessary to identify the alveolar duct. (3) The enzymatic and microfluidic isolation of single cells allowed for the harvest of as few as several thousand cells for PCR analysis. Microfluidics based arrays were used to measure the expression of selected marker genes in individual cells to characterize different cell populations. Preliminary work suggests the unique value of this approach to understand the intra- and intercellular interactions within the regenerating alveolar duct.

Keywords: single-cell analysis, laser microdissection, microfluidics, alveolar duct, murine lung gene expression, signaling network, regenerative medicine

INTRODUCTION

Complex tissues such as the lung are composed of structural hierarchies such as alveoli, alveolar ducts, and lobules (1). Recent evidence indicates that these structures reflect not only mechanical relationships, but also functional units that selectively participate in integrated processes such as tissue regeneration (2) and the development of bronchioalveolar carcinoma (3). Because bulk analyses of cells and gene expression – ignoring these regenerative units – have failed to illuminate the interactions between cells participating in these processes (4, 5), there is growing interest in the spatial sampling of the cells within regenerative units.

The initial attempts to refine the bulk analysis of cells within regenerating tissues used flow cytometry (FC) (6). FC is a multi-dimensional high-throughput technology that can analyze and sort individual cells based on their phenotypic characteristics – in most cases, sorting is based on cell surface molecule expression (7, 8). This approach has provided useful insights into the molecular expression of cell populations participating in lung regeneration (9–12); nonetheless, the relatively large number of cells sorted by FC has potentially obscured the cell–cell interactions within individual regenerative units.

To address these limitations, there is growing interest in isolating cells within individual regenerative units; in lung regeneration, the anatomic unit appears to be the alveolar duct. This goal has been aided by two developments. First, computer-controlled laser microdissection of tissue has facilitated the rapid isolation of small anatomic units within complex tissues. The ability to harvest anatomic units, such as the alveolar duct, under physiologic conditions has enabled detailed single-cell analysis. Second, microfluidic devices capable of capturing and handling single cells allowed for the analysis of the small number of cells comprising anatomic units such as the alveolar duct. Furthermore, these isolated cells can now be analyzed for gene expression at the level of individual cells. The result is an opportunity to define not only the signaling interactions between cells, but also the molecular interactions and signaling pathways within cells (9, 11, 13).

In this report, we demonstrate the use of laser microdissection to isolate cells in the murine lung alveolar duct and the microfluidic isolation and gene expression analysis of individual cells within this structural unit.

MATERIALS AND METHODS

ANIMALS

Male mice, 8–10-week-old wild type C57BL/6 (Jackson Laboratory, Bar Harbor, ME, USA) were anesthetized as previously described (14). The care of the animals was consistent with guidelines of the American Association for Accreditation of

Abbreviations: 2D, 2-dimensional; 3D, 3-dimensional; IR, infrared; LCM, laser capture microdissection; PCR, polymerase chain reaction; PEN, polyethylene naphthalene; SEM, scanning electron microscopy; UV, ultraviolet; SCA, single-cell analysis; SD, standard deviation.

Laboratory Animal Care (Bethesda, MD, USA) and approved by our Institutional Animal Care and Use Committee.

ANESTHESIA AND INTUBATION

The animals were anesthetized with an intraperitoneal injection of ketamine 100 mg/kg (Fort Dodge Animal Health, Fort Dodge, IA, USA) and xylazine 6 mg/kg (Phoenix Scientific, Inc., St. Joseph, MO, USA). The animals were intubated under direct visualization with a standard 20 g angiocatheter (BD Insyte, Sandy, UT, USA) (14) for subsequent agarose instillation.

CORROSION CASTING AND SEM

The right ventricular outflow tract was cannulated via right ventriculotomy with a 2 mm olive-tipped cannula (Acufirm 1428LL, Dreieich, Germany). The pulmonary vessels were perfused with 15–20 ml of 37°C saline followed by a buffered 2.5% glutaraldehyde solution (Sigma, St Louis, MO, USA) at pH 7.40. After casting of the pulmonary microcirculation with PU4ii (VasQtec, Zurich, Switzerland), diluted with 20% methylmethacrylate monomers (Sigma), and caustic digestion, the microvascular corrosion casts were imaged after coating with gold in an argon atmosphere with a Philips ESEM XL30 scanning electron microscope as previously described (13).

EMBEDDING MEDIUM

Agarose at 3% (w/v) was thoroughly mixed with distilled H₂O and warmed to 37°C. The trachea, cannulated with a 20 g Angiocath (BD Insyte), was infused with the 37°C agarose using the lowest pressure necessary to inflate the peripheral lung (typically 20 cm H₂O pressure). At total lung capacity, the trachea was clamped and the lung block was placed in 4°C saline and allowed to harden.

PRECISION-CUT LUNG SLICES

Sectioning was performed with the Leica VT1000 S vibrating blade microtome (Leica Biosystems, Nussloch, Germany) using stainless steel razor blades (Gillette, Boston, MA, USA). The microtome was operated at the following adjustable settings: knife angle, 5–7°; sectioning speed, 0.05–0.2 mm/s; oscillation frequency, 80–100 Hz; and oscillation amplitude, 0.6 mm. Most sections were 200 μm thick and mounted on a polyethylene naphthalate (PEN) membrane frame slide (Life Technologies, Carlsbad, CA, USA). The precision-cut lung slices were immersed in Dulbecco's Modified Eagle's Medium (DMEM) (Cellgro, Herndon, VA, USA) at 4°C prior to laser microdissection.

LASER MICRODISSECTION

The Arcturus XT LCM System (Life Technologies) was used for all ultraviolet (UV) laser dissection. The UV laser was a specially adapted beta-test laser for wet tissue applications. The enhanced UV cutting laser was a solid-state, diode-pumped (345 nm) laser with adjustable current (0–100%) and pulse frequency (10–5000 Hz). After mounting on the Arcturus stage, the surface of the lung slice was blotted dry. The alveolar ducts were optically targeted using a Nikon Eclipse Ti-E microscope with 10× and 20× Nikon CF objectives with high-intensity LED illumination. The stage was adjusted using a motorized trackball actuated in X- and Y-axes with 1 μm precision. The UV laser was empirically

adjusted between 30 and 50% of maximal current to ensure complete penetration of the tissue slice. The Arcturus XT software was used to target tissue for UV dissection.

ENZYMATIC DIGESTION

Enzymatic digestion of the lung reflected a previously published protocol (15). Briefly, collagenase Type IV and DNase I (Sigma) was used to dissociate the tissue. The digestion was performed at 37°C under constant agitation until dissolved. The digest was filtered through 35 μm nylon mesh in preparation for microfluidic analysis.

CELL VIABILITY

BAL-derived cells were counted using a Neubauer hemacytometer (Fisher, Pittsburgh, PA, USA). Dead cells were excluded by trypan blue (Sigma, St. Louis, MO, USA). Viability was further assessed using the calcein and ethidium live/dead assay (16) and measured by microfluorimetry (CytoFluor 4000, Applied Biosystems, Foster City, CA, USA) (17).

C1 MICROFLUIDICS CHIP

The C1 single-cell auto prep array integrated fluidic circuit (chip) is the microfluidic component of the Fluidigm C1™ Single-Cell Auto Prep System. The medium chip (10–17 μm cell size) was used to capture single cells (96 on one chip) obtained from the laser microdissection. The chip was used to perform single-cell PCR using a custom 96 gene panel designed for the alveolar duct.

FLOW CYTOMETRY

After standard enzymatic digestion of the lung (10), FC cell sorting using anti-CD31 mAb (APC or PE-Cy7; rat IgG2a, clone 390, eBioScience) (18) was used to isolate the CD31⁺ endothelial cells. Endothelial cell gene expression was assessed by PCR array as previously described (6).

PCR GENE EXPRESSION

Comparison of single-cell and FC values were based on Ct values (6). For population analyses, the gene expression based on the ΔCt method (19) used an average of five housekeeping genes. The ΔCt values were normalized to an arbitrary 100-point linear scale for comparison with single-cell values.

RESULTS

PRECISION-CUT LUNG SLICES

Structural analysis of the murine lung using SEM demonstrated a mean diameter of the intact alveolar duct of 177 ± 31 μm (Figure 1). To obtain thickness-calibrated lung slices encompassing the alveolar ducts, 200 μm thick precision-cut lung slices were sectioned after intra-airway instillation of a 3% (w/v) agarose embedding medium. At 37°C, low melting point agarose had sufficiently low viscosity to permit instillation into the peripheral airspaces – important for the preservation of alveolar architecture. When cooled to 4°C, the agarose-lung block demonstrated stability for precision sectioning. The agarose-lung block, mounted on Leica VT1000 S specimen holder and immersed in ice-cold PBS, was serially sectioned (Figure 2). For single-cell genomics studies, the lung slices were mounted on a PEN membrane frame slide to

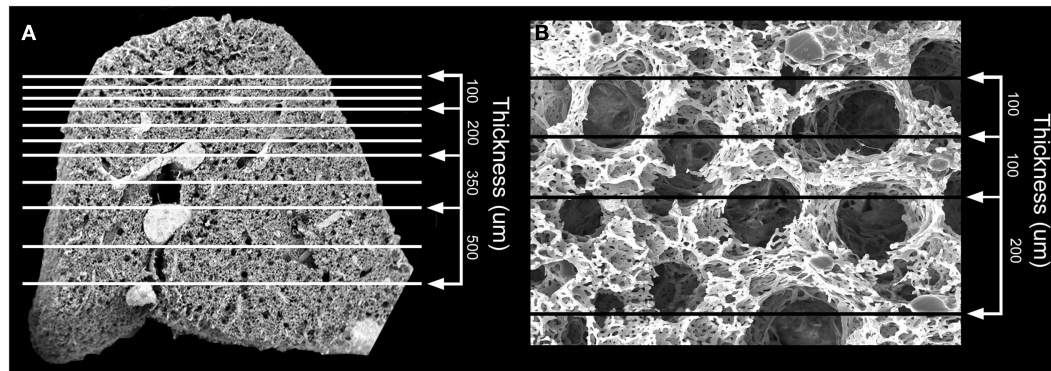


FIGURE 1 | Scanning electron microscopy (SEM) of the polymer casted murine lung. (A) Cross-sectional 12x SEM of murine lung including representative size measurements at right. Vascular fixation and casting – the method with the least shrinkage of common lung preparation

techniques – demonstrated bronchiolar and alveolar duct architecture when examined by SEM. **(B)** 200x SEM image of murine lung demonstrating size of alveolar ducts. The alveolar ducts were demonstrably contained within the 200 μm tissue slice.

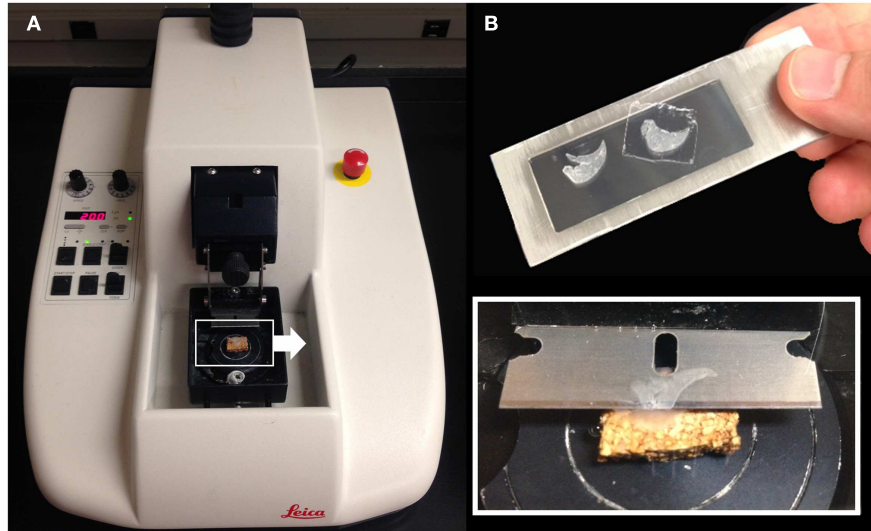


FIGURE 2 | Precision-cut lung slices were obtained by a vibrating blade microtome after agarose embedding (A). The agarose-lung block was initially mounted on a cork specimen platform with cyanoacrylate prior to

sectioning (inset). The cut sections were subsequently mounted on a frame slide with a PEN membrane used for standard laser capture microdissection **(B)**.

provide structural support during laser dissection. The frame slide facilitated the retrieval and subsequent processing of the dissected specimen **(Figure 3)**.

OPTICAL TARGETING

The hierarchical anatomic structure of the lung facilitated the visual identification of the alveolar duct. The dehydrated lung used in laser capture loses structural detail when examined by light microscopy (not shown). In contrast, the well-hydrated lung used in laser microdissection – in the absence of counterstains or cell-specific labels – retains structural detail throughout the 200–300 μm thick precision-cut lung slices **(Figure 4)**. Preliminary identification of the alveolar duct was confirmed by varying the optical plane and identifying the feeding bronchiole

(Figures 4A,B). The computer-controlled laser software allowed for precise selection of regions encompassing the alveolar duct; the demarcated regions were harvested by the UV cutting laser **(Figures 4C,D)**. The laser power, speed, and focal point were varied to optimize single-pass dissection of the tissue and minimize thermal damage. The required laser power was consistently reduced by 50% with absorbent blotting of the section surface followed by re-application of media immediately following UV dissection.

SINGLE-CELL ISOLATION

The laser-dissected samples were enzymatically digested, micro-filtered, and prepared for microfluidic analysis **(Figure 5)**. The PEN membrane-associated samples were incubated in collagenase

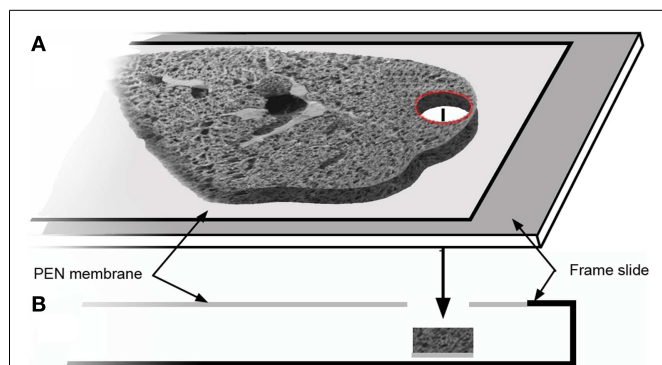


FIGURE 3 | The tissue slice was mounted on a frame slide. The slide is composed of a standard optical microscope slide with a metal frame that supports a PEN membrane to facilitate laser microdissection (A). In cross-section (B), the frame slide creates a reservoir for retrieval of the dissected tissue.

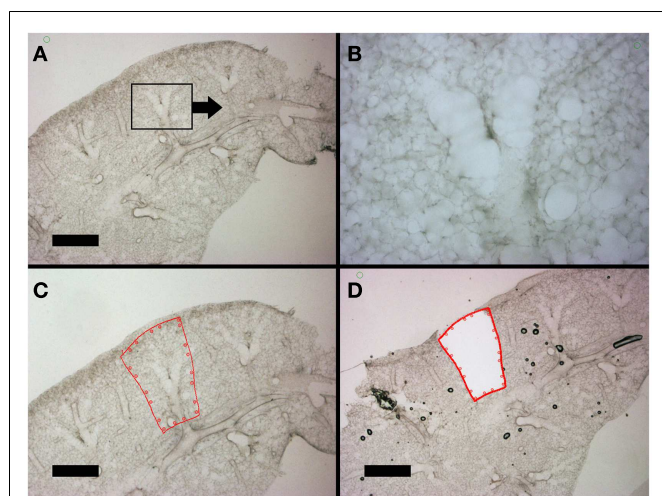


FIGURE 4 | Lung slices of the murine cardiac lobe examined by light microscopy. After mounting on a frame slide, the sections were visualized without counter-stain at 10× (A,C,D) and 20× (B) magnification. The respiratory bronchiole and alveolar ducts were readily identified (B). The relevant anatomic structure was demarcated by software annotation (C) and laser microdissected using computer control (D). Successful dissection is demonstrated as the structure drops into the frame slide and out of the optical plane (D). Bar = 1 mm.

Type IV buffer for 15–30 min at 37°C with constant agitation. The acellular matrix and PEN membrane-associated debris were microfiltered with a 35 μm mesh. Routine examination of the filtered debris demonstrated virtually no residual cells. Cell yields varied from 1 to 3×10^3 cells per alveolar duct. Cell viabilities, assessed by vital dye exclusion as well as live/dead assay microfluorimetry, ranged from 70 to 95% depending on treatment conditions. Live/dead confocal microscopy demonstrated dead cells at the laser-dissected sample margins (not shown), but cell viability from laser-dissected tissue (87 ± 5) was not statistically different from enzymatic digestion alone (95 ± 4) ($p > 0.05$). The cells were analyzed using the Fluidigm C1™ Single-Cell Auto Prep

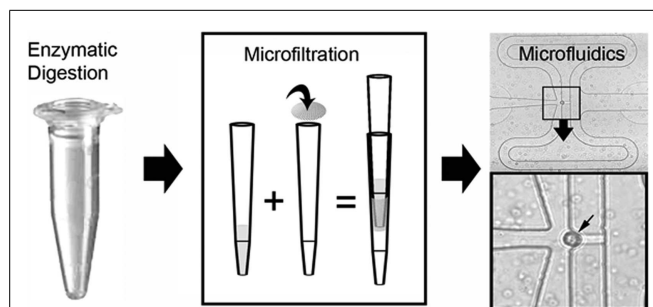


FIGURE 5 | Schematic of the single-cell isolation procedure after laser microdissection. The tissue samples were enzymatically digested and microfiltered using a 35 μm mesh. Single cells were isolated and PCR performed on a C1 microfluidics chip. The successful capture of individual cells was readily identified by light microscopy (inset, small arrow).

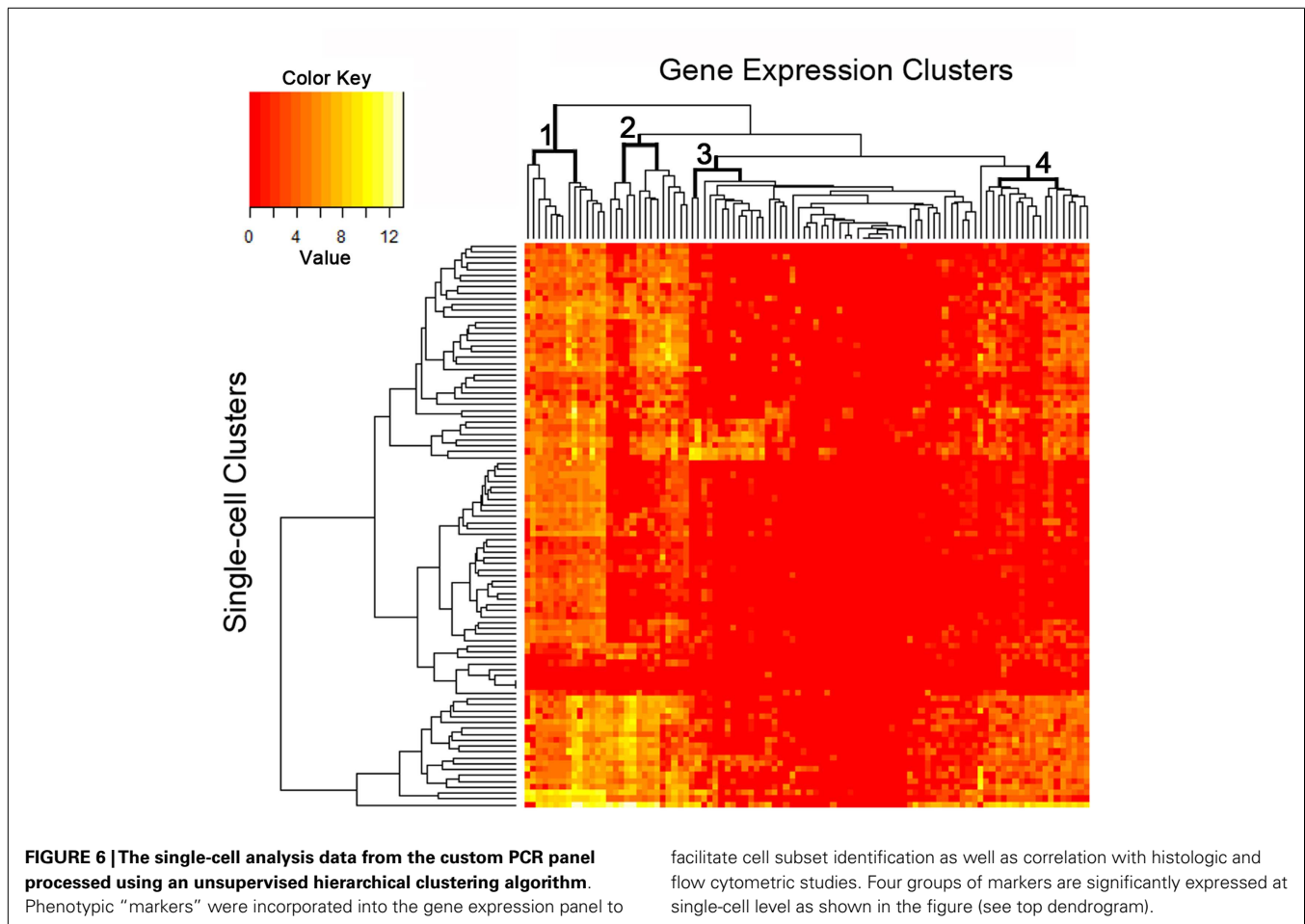
System (Fluidigm, South San Francisco, CA, USA). In the 96-well C1 system, a typical result was the capture of 75 single cells, 13 wells with 2 or more cells, and 2 wells with no cells.

SINGLE-CELL PCR

The C1 chip used a microfluidic circuit to capture the isolated single cells (96 on one chip). The single-cell poly-adenylated RNA was converted to full-length cDNA for universal amplification of the cDNA and custom PCR analysis. Our custom PCR arrays were developed based on gene expression studies using FC-based phenotypic isolation of lung cells (6, 10–12, 20). Results of the C1 PCR studies were analyzed by unsupervised hierarchical clustering (Figure 6). Upon filtering based on array QC readouts, data on 72 single-cells were available. In addition, we have eliminated the genes that showed low variation (SD less than 1) followed by feature selection. Thus, we obtained a smaller matrix of 72 single-cells \times 42 marker genes. Clustering based on selected features (using the Sparse Hierarchical Clustering module in GenePattern software from Broad Institute of MIT) demonstrated single-cell clusters (Figure 7) that corresponded to previously identified cell types (e.g., endothelial cells, myofibroblasts, alveolar macrophages, and alveolar epithelial cells). The information content of single-cell analysis was apparent when gene expression of endothelial cells (*Pecam1* gene expression) isolated by the C1 chip was compared to gene expression of endothelial cells (CD31⁺ surface expression) isolated by FC. Although the expression of many genes was similar in both groups (Figure 8A), some genes demonstrated variable expression patterns that were not reflected in the population-based FC analysis (Figure 8B).

DISCUSSION

In this report, we demonstrated laser microdissection of the lung alveolar duct for single-cell PCR analysis. Our approach involved three steps. (1) The initial preparation used mechanical sectioning of the lung tissue with sufficient thickness to encompass the structure of interest. In the case of the alveolar duct, the precision-cut lung slices were 200 μm thick and processed using near-physiologic conditions to preserve cell viability. (2) The lung slices were examined by transmission light microscopy to target the alveolar duct. The air-filled lung was sufficiently accessible

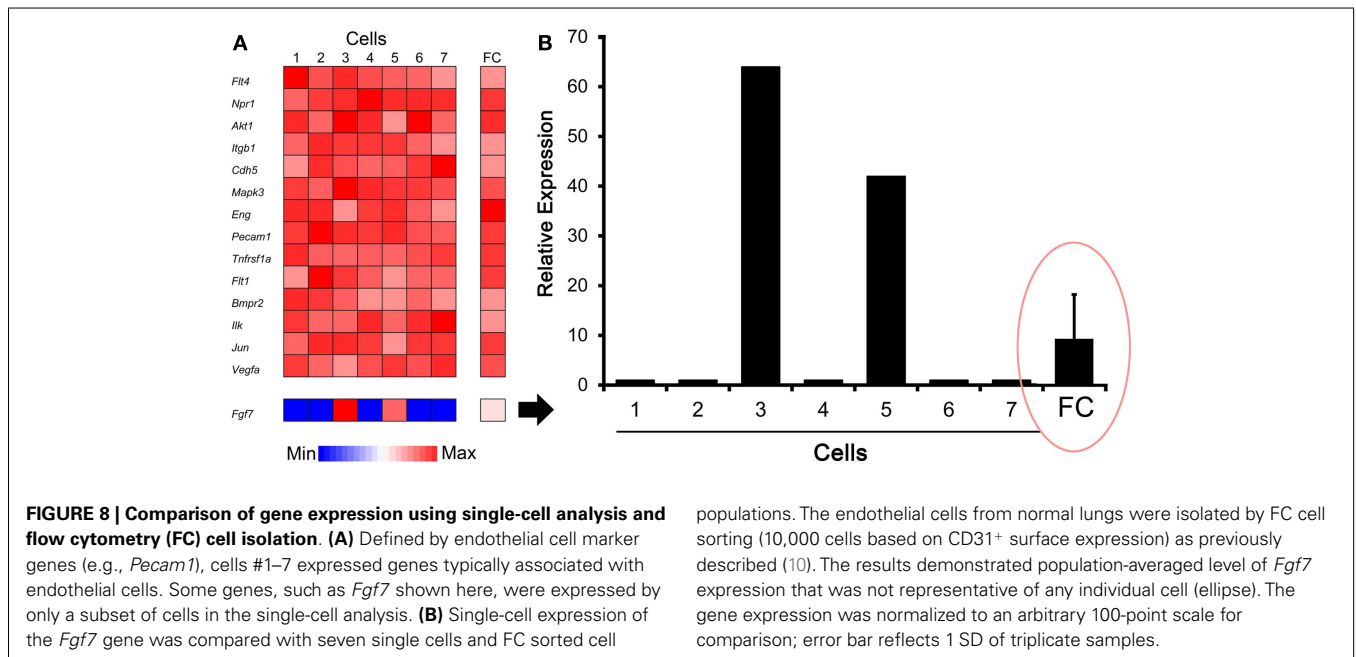
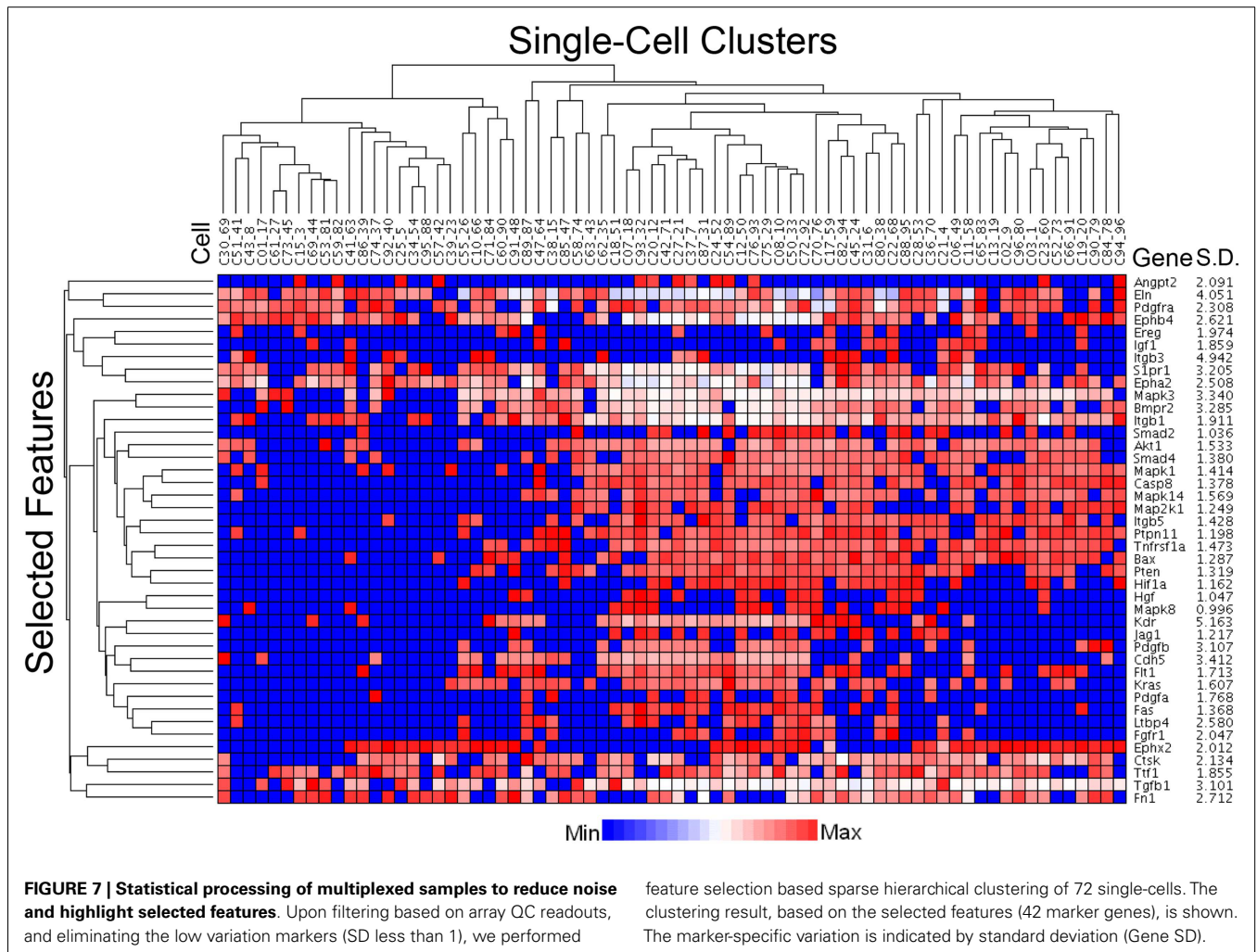


by light microscopy that counterstains or fluorescent labels were unnecessary to identify the alveolar duct. (3) The enzymatic and microfluidic isolation of single cells for PCR allowed for the harvest of as few as several thousand cells for analysis. The data suggest the unique value of this approach to understanding the intra- and intercellular interactions within the regenerating or neoplastic alveolar duct.

Harvesting viable cells from the alveolar duct requires that tissue slices of the appropriate thickness have to be obtained in near-physiologic conditions. Manually sliced tissues have been used for nearly 90 years in various *in vitro* applications (21, 22); however, the manually prepared slices have had limited reproducibility and viability (23). A mechanical tool to facilitate the cutting of tissue of precise thickness was introduced by the Krumdieck in 1980 (24, 25). With progressive refinement, tissue microtomes now vibrate with varying amplitudes and frequencies to produce slices with highly reproducible thickness – thus, these sections are referred to as precision-cut tissue slices (26). With current vibrating microtomes, precision-cut tissue slices preserve the original organ architecture, the cellular heterogeneity, and extracellular matrix found *in vivo* (27). Precision-cut tissue slices, for example, have enabled the development of *ex vivo* systems for systematic pharmacokinetic profiling of tumors contained in their native 3-dimensional micro-environment (28).

A key feature of precision-cut lung slices in the lung is the use of agarose as structural support. Because live tissue is too soft for precise sectioning, and molten paraffin is too hot for live tissue, a biocompatible liquid with a low-temperature gelling point is used as an embedding medium. Agarose is typically used for lung embedding because it has sufficiently low viscosity at 37–40°C to be infused into the distal airspaces, yet is sufficiently rigid for microtome sectioning at 4°C.

Although there is a significant overlap between techniques, laser microdissection can be distinguished from laser capture microdissection (LCM) by the method of cell isolation. In the original LCM system developed at the National Institutes of Health, the target cells were identified by light microscopy and captured using an infrared laser (29). A transfer film positioned over the region of interest (typically tumor cells) was melted into the tissue using an IR laser. The dissected tissue microsample was then lifted from the histopathology slide for subsequent RNA, DNA, or protein analysis. In most contemporary LCM systems, a requirement for effective capture is the dehydration of the tissue – a requirement that precludes the study of live cells (30). In contrast, our laser microdissection approach uses a cutting UV laser to define the margins of the dissection under near-physiologic conditions. Although UV-induced thermal injury to the neighboring cells is demonstrable using live-dead assays; the dissection margins can be



drawn to minimize the injury to the region of interest. In our application, we maintained near-physiologic conditions during the UV laser dissection with only blotting of the tissue surface to minimize excess liquid media prior to UV dissection. The UV laser-defined alveolar duct was subsequently transferred to the collection chamber without the use of an IR laser or transfer film; in most cases, the sample dropped into the chamber occasionally assisted by the application of liquid media.

A frequently under-appreciated characteristic of the lung is the large amount of extracellular matrix in the organ (31). In addition, some extracellular matrix components – most notably, elastin – are resistant to common enzymatic treatments (32). In our application, we have used a variety of enzymatic cocktails based on collagenase to facilitate dissolution of the laser-dissected tissue; however, the most important component has proven to be collagenase Type IV. In our protocols, we used 35- μ m mesh to separate cells from the collagenase-resistant matrix debris. Routine re-examination of the filtered debris did not show residual cells suggesting that this approach does not result in the systematic loss of any particular cell subpopulation. Of note, cell filtration with mesh larger than 35 μ m was prone to debris-induced occlusion of the microfluidics chip.

The cells isolated by microfluidics were studied using a custom 96 gene PCR panel. The results of prior FC population studies were used to select the genes used in this custom panel (6, 9–12, 20). FC-derived cell type-specific markers were incorporated into the panel to facilitate the spatial reconstruction of intercellular interactions within the alveolar duct. For example, the genes *Acta2* and *Pecam1* were added to the PCR panel to identify myofibroblasts and endothelial cells, respectively. Although the single-cell transcriptional data must be analyzed in the context of potential limitations, such as burst transcription (33, 34), insights derived from these data should be useful for re-interpreting population-based data both *in vivo* and *in vitro*.

Single-cell analysis is particularly relevant to the process of carcinogenesis within the alveolar duct. Bronchioalveolar stem cells, in addition to contributing to the maintenance and repair of the normal alveolar duct, have been shown to give rise to lung adenocarcinomas (35). The experimental challenge is that multipotent stem cells, like those giving rise to bronchioalveolar carcinoma, exist in low frequency within the peripheral lung. Population-based analyses are prone to overlook these cells and their transcriptional profile because of the “averaging” effect demonstrated in our study. Because of this limitation, we anticipate that single-cell analysis of the regenerating alveolar duct will provide important insights into the biology of bronchioalveolar stem cells.

Finally, these results demonstrate the ability to extract viable cells from a morphologically defined micro-region of a tissue sample. We successfully applied single-cell whole-transcriptome amplification and gene expression analyses to these samples – a process that allows for simultaneous region-specific and cell type-specific expression analysis. We anticipate even more interesting experiments are possible in the future. For example, similarly obtained viable single cells can facilitate a variety of experimental perturbations prior to endpoint analyses (e.g., expression profiling, nucleic acid sequencing, immunoassays, or proteomics). Furthermore, new statistical and bioinformatics techniques may

be used to design efficient strategies for sampling cells at different locations in the tissue and at different time-points, and to study the genomics and transcriptomics of these cellular samples, thus leading to construction of spatio-temporal cell signaling networks. We are confident that such studies involving single-cell analysis will lead to a more nuanced understanding of the process of tissue regeneration.

ACKNOWLEDGMENTS

Supported in part by NIH Grants HL94567 and CA009535. Saumyadipta Pyne was supported by Ramalingaswami-DBT Fellowship, DST CMS, and MoS&PI India. (Project No. SR/SA/MS:516/07 dated 21/04/2008).

SUPPLEMENTARY MATERIAL

The Supplementary Material for this article can be found online at <http://www.frontiersin.org/Journal/10.3389/fonc.2014.00260/abstract>

REFERENCES

1. Weibel ER, Gomez DM. Architecture of the human lung. *Science* (1962) **137**:577–85. doi:10.1126/science.137.3530.577
2. Weibel ER. How to make an alveolus. *Eur Respir J* (2008) **31**:483–5. doi:10.1183/09031936.00003308
3. Yanagi S, Kishimoto H, Kawahara K, Sasaki T, Sasaki M, Nishio M, et al. Pten controls lung morphogenesis, bronchioalveolar stem cells, and onset of lung adenocarcinomas in mice. *J Clin Invest* (2007) **117**:2929–40. doi:10.1172/jci31854
4. Paxson JA, Parkin CD, Iyer LK, Mazan MR, Ingenito EP, Hoffman AM. Global gene expression patterns in the post-pneumonectomy lung of adult mice. *Respir Res* (2009) **10**:1–15. doi:10.1186/1465-9921-10-92
5. Wolff JC, Wilhelm J, Fink L, Seeger W, Voswinckel R. Comparative gene expression profiling of postnatal and post-pneumonectomy lung growth. *Eur Respir J* (2009) **28**:28. doi:10.1183/09031936.00059709
6. Lin M, Chamoto K, Gibney B, Lee GS, Collings-Simpson D, Houdek J, et al. Angiogenesis gene expression in murine endothelial cells during post-pneumonectomy lung growth. *Respir Res* (2011) **12**:98. doi:10.1186/1465-9921-12-98
7. Zeng QT, Pratt JP, Pak J, Ravnich D, Huss H, Mentzer SJ. Feature-guided clustering of multi-dimensional flow cytometry datasets. *J Biomed Inform* (2007) **40**:325–31. doi:10.1016/j.jbi.2006.06.005
8. Rossin E, Lin T-I, Hsiu JH, Mentzer SJ, Pyne S. A framework for analytical characterization of monoclonal antibodies based on reactivity profiles in different tissues. *Bioinformatics* (2011) **27**:2746–53. doi:10.1093/bioinformatics/btr468
9. Chamoto K, Gibney BC, Ackermann M, Lee GS, Lin M, Konerding MA, et al. Alveolar macrophage dynamics in murine lung regeneration. *J Cell Physiol* (2012) **227**:3208–15. doi:10.1002/jcp.24009
10. Chamoto K, Gibney BC, Lee GS, Lin M, Simpson DC, Voswinckel R, et al. CD34+ progenitor to endothelial cell transition in post-pneumonectomy angiogenesis. *Am J Respir Cell Mol Biol* (2012) **46**:283–9. doi:10.1165/rcmb.2011-0249OC
11. Chamoto K, Gibney BC, Ackermann M, Lee GS, Konerding MA, Tsuda A, et al. Alveolar epithelial dynamics in post-pneumonectomy lung growth. *Anat Rec (Hoboken)* (2013) **296**:496–503. doi:10.1002/ar.22659
12. Chamoto K, Gibney BC, Lee GS, Ackermann M, Konerding MA, Tsuda A, et al. Migration of CD11b+ accessory cells during murine lung regeneration. *Stem Cell Res* (2013) **10**:267–77. doi:10.1016/j.scr.2012.12.006
13. Konerding MA, Gibney BC, Houdek J, Chamoto K, Ackermann M, Lee G, et al. Spatial dependence of alveolar angiogenesis in post-pneumonectomy lung growth. *Angiogenesis* (2012) **15**:23–32. doi:10.1007/s10456-011-9236-y
14. Gibney B, Lee GS, Houdek J, Lin M, Chamoto K, Konerding MA, et al. Dynamic determination of oxygenation and lung compliance in murine pneumonectomy. *Exp Lung Res* (2011) **37**:301–9. doi:10.3109/01902148.2011.561399
15. van Beijnum JR, Rousch M, Castermans K, Van Der Linden E, Griffioen AW. Isolation of endothelial cells from fresh tissues. *Nat Protoc* (2008) **3**:1085–91. doi:10.1038/nprot.2008.71

16. Papadopoulos NG, Dedoussis GV, Spanakos G, Gritzapis AD, Baxevasis CN, Papamichail M. An improved fluorescence assay for the determination of lymphocyte-mediated cytotoxicity using flow cytometry. *J Immunol Methods* (1994) **177**:101–11. doi:10.1016/0022-1759(94)90147-3
17. Su M, He C, West CA, Mentzer SJ. Cytolytic peptides induce biphasic permeability changes in mammalian cell membranes. *J Immunol Methods* (2001) **252**:63–71. doi:10.1016/S0022-1759(01)00334-9
18. Baldwin HS, Shen HM, Yan H-C, Delisser HM, Chung A, Mickanin C, et al. Platelet endothelial cell adhesion molecule-1 (PECAM-1/CD31): alternatively spliced, functionally distinct isoforms expressed during mammalian cardiovascular development. *Development* (1994) **120**:2539–53.
19. Livak KJ, Schmittgen TD. Analysis of relative gene expression data using real-time quantitative PCR and the 2(-Delta Delta C(T)) method. *Methods* (2001) **25**:402–8. doi:10.1006/meth.2001.1262
20. Chamoto KB, Gibney M, Lin GS, Lee D, Collings-Simpson J, Houdek MA, et al. *Regulatory Network of Angiogenesis Gene Expression during Post-Pneumonectomy Compensatory Growth*. Denver, CO: American Thoracic Society (2011).
21. Warburg O. Versuche an uberlebendem karzinomgewebe. *Biochem Z* (1923) **142**:317–33.
22. Graaf IA, Groothuis GM, Olinga P. Precision-cut tissue slices as a tool to predict metabolism of novel drugs. *Expert Opin Drug Metab Toxicol* (2007) **3**:879–98. doi:10.1517/17425255.3.6.879
23. Olinga P, Meijer DK, Slooff MJ, Groothuis GM. Liver slices in in vitro pharmacotoxicology with special reference to the use of human liver tissue. *Toxicol In vitro* (1998) **12**:77–100. doi:10.1016/s0887-2333(97)00097-0
24. Krumdieck CL, Dossantos JE, Ho KJ. A new instrument for the rapid preparation of tissue-slices. *Anal Biochem* (1980) **104**:118–23. doi:10.1016/0003-2697(80)90284-5
25. Krumdieck CL. Development of a live tissue microtome: reflections of an amateur machinist. *Xenobiotica* (2013) **43**:2–7. doi:10.3109/00498254.2012.724727
26. Morin JB, Baste JM, Gay A, Crochemore C, Corbiere C, Monteil C. Precision cut lung slices as an efficient tool for in vitro lung physio-pharmacotoxicology studies. *Xenobiotica* (2013) **43**:63–72. doi:10.3109/00498254.2012.727043
27. Fahy GM, Guan N, De Graaf IA, Tan Y, Griffin L, Groothuis GM. Cryopreservation of precision-cut tissue slices. *Xenobiotica* (2013) **43**:113–32. doi:10.3109/00498254.2012.728300
28. Vaira V, Fedele G, Pyne S, Fasoli E, Zadra G, Bailey D, et al. Preclinical model of organotypic culture for pharmacodynamic profiling of human tumors. *Proc Natl Acad Sci U S A* (2010) **107**:8352–6. doi:10.1073/pnas.0907676107
29. Emmert-Buck MR, Bonner RF, Smith PD, Chuaqui RF, Zhuang Z, Goldstein SR, et al. Laser capture microdissection. *Science* (1996) **274**:998–1001. doi:10.1126/science.274.5289.998
30. Vandewoestyne M, Goossens K, Burvenich C, Van Soom A, Peelman L, Deforce D. Laser capture microdissection: should an ultraviolet or infrared laser be used? *Anal Biochem* (2013) **439**:88–98. doi:10.1016/j.ab.2013.04.023
31. Badylak SF. The extracellular matrix as a biologic scaffold material. *Biomaterials* (2007) **28**:3587–93. doi:10.1016/j.biomaterials.2007.04.043
32. Duca L, Floquet N, Alix AJ, Haye B, Debelle L. Elastin as a matrikine. *Crit Rev Oncol Hematol* (2004) **49**:235–44. doi:10.1016/j.critrevonc.2003.09.007
33. Livak KJ, Wills QF, Tipping AJ, Datta K, Mittal R, Goldson AJ, et al. Methods for qPCR gene expression profiling applied to 1440 lymphoblastoid single cells. *Methods* (2013) **59**:71–9. doi:10.1016/j.ymeth.2012.10.004
34. Wills QF, Livak KJ, Tipping AJ, Enver T, Goldson AJ, Sexton DW, et al. Single-cell gene expression analysis reveals genetic associations masked in whole-tissue experiments. *Nat Biotechnol* (2013) **31**:748–53. doi:10.1038/nbt.2642
35. Kim CF, Jackson EL, Woolfenden AE, Lawrence S, Babar I, Vogel S, et al. Identification of bronchioalveolar stem cells in normal lung and lung cancer. *Cell* (2005) **121**:823–35. doi:10.1016/j.cell.2005.03.032

Conflict of Interest Statement: The authors declare that the research was conducted in the absence of any commercial or financial relationships that could be construed as a potential conflict of interest.

Received: 24 May 2014; accepted: 06 September 2014; published online: 24 September 2014.

Citation: Bennett RD, Ysasi AB, Belle JM, Wagner WL, Konerding MA, Blainey PC, Pyne S and Mentzer SJ (2014) Laser microdissection of the alveolar duct enables single-cell genomic analysis. *Front. Oncol.* **4**:260. doi: 10.3389/fonc.2014.00260

This article was submitted to *Molecular and Cellular Oncology*, a section of the journal *Frontiers in Oncology*.

Copyright © 2014 Bennett, Ysasi, Belle, Wagner, Konerding, Blainey, Pyne and Mentzer. This is an open-access article distributed under the terms of the Creative Commons Attribution License (CC BY). The use, distribution or reproduction in other forums is permitted, provided the original author(s) or licensor are credited and that the original publication in this journal is cited, in accordance with accepted academic practice. No use, distribution or reproduction is permitted which does not comply with these terms.